A Proposed Model for Breakthrough Curves of Methylene Blue Adsorption on Biochar

H. D. Tran,[a] H. N. Phuc,[b] P. V. H. Phuong,[c] L. N. P. Thien,[d,e] T. L. Nguyen,[f,g] U. P. N. Tran,[h] and V.-H. Dang[i,e,*]

[a]Faculty of Environment, Ho Chi Minh University of Natural Resources and Environment, Ho Chi Minh City, Vietnam

[b]Office of R&D and External Relations, Ho Chi Minh University of Natural Resources and Environment, Ho Chi Minh City, Vietnam

[c]Faculty of Meteorology and Climate Change, Ho Chi Minh University of Natural Resources and Environment, Ho Chi Minh City, Vietnam

[d]Laboratory of Biofuel and Biomass Research, Faculty of Chemical Engineering, Ho Chi Minh City University of Technology (HCMUT), 268 Ly Thuong Kiet, District 10, Ho Chi Minh City, Vietnam

[e]Vietnam National University Ho Chi Minh City, Linh Trung Ward, Thu Duc City, Ho Chi Minh City, Vietnam

[f]Institute of Fundamental and Applied Sciences, Duy Tan University, Ho Chi Minh City, Vietnam

[g]Faculty of Environmental and Chemical Engineering, Duy Tan University, Da Nang City, Vietnam

[h]Faculty of Engineering and Technology, Van Hien University, Ho Chi Minh City, Vietnam

[i]Faculty of Chemical Engineering, Ho Chi Minh City University of Technology (HCMUT), 268 Ly Thuong Kiet, District 10, Ho Chi Minh City, Vietnam

doi: https://doi.org/10.15255/CABEQ.2023.2280

Original scientific paper
Received: December 16, 2023
Accepted: April 3, 2024

Dye pollutants, mainly discharged from the textile industry, have caused severe risks to human health and the ecosystem because of their toxicity, non-biodegradability, and carcinogenicity. This study investigated the use of commercial biochar derived from melaleuca wood as an adsorbent for the removal of methylene blue (MB) using a packed-bed column. The selected biochar was characterized by nitrogen adsorption-desorption isotherms, Fourier transform infrared spectroscopy, and scanning electron microscopy. The experiments were performed to determine breakthrough curves (BTCs) with varying pH (3–9), inflow rate (5–20 mL min^{-1}), bed height (16–65 cm), and initial MB concentration (0.75–9 mg L^{-1}). The biochar (particle size of 1–2 mm) exhibited a low adsorption capacity for MB (~21 mg kg^{-1}), resulting in a short breakthrough time. The Thomas, Bohart-Adams, Yoon-Nelson, and Bed Depth Service Time models were quite suitable for describing the experimental BTCs, with R^2-values ranging from 0.92 to 0.98. The obtained BTCs were not in the typical S-shape, which characterizes diffusion-controlled adsorption. Therefore, a serial logistic-exponential model, which accounts for both the mass transfer and interaction contributions, was proposed. The experimental data effectively fit this proposed model, as indicated by high R^2-values (>0.998). The dominant influence of mass transfer compared to interaction in controlling the adsorption rate of MB was highlighted.

Keywords
continuous adsorption, breakthrough curve, dye removal, biochar adsorbent

Introduction

Methylene blue (MB) is a colored pollutant commonly found in wastewater discharged from textile industries. MB poses significant risks to human health and the environment due to its toxicity, carcinogenic properties, and poor biodegradability[1–3]. MB can cause the death of premature cells in tissues, skin and eye irritations, and serious serotonin toxicity[1,2]. Various techniques are employed for removing dyes from wastewater, including membrane processes[4,5], chemical oxidation processes[6,7], biological processes[8,9], and physiochemical techniques, primarily adsorption[10,11]. In an aqueous

*Corresponding author, e-mail: dvhan@hcmut.edu.vn

environment, the presence of MB can inhibit microorganism activity due to its high light absorbance, resulting in limited efficiency of biological and photocatalytic degradation[12]. Adsorption, being a potentially effective and convenient method for MB removal, offers advantages such as high efficiency, low cost, flexibility, and the availability of adsorbent precursors[1,13,14].

Biochar is considered a low-cost and environmentally friendly adsorbent for wastewater treatment. Both modified and unmodified biochars have been studied for their ability to adsorb MB[15,16]. Raw biochars derived from various sources have been utilized to adsorb MB, resulting in varied adsorption capacities, such as 4.58 mg g^{-1} for sawdust biochar[17], 8.07 mg g^{-1} for rice husk biochar[18], and 3.99 mg g^{-1} for pine wood biochar[19]. To improve the adsorption efficiency of biochar, activation or modification techniques can be applied. For example, chemical activation of lychee seed biochar can increase the MB adsorption capacity to 124.5 mg g^{-1} [20]. Recently, Hassaan *et al*.[21] prepared sawdust biochar modified by ozone-triethylenetetramine for MB adsorption, achieving an adsorption capacity of 568.16 mg g^{-1}.

To the best of our knowledge, previous research has primarily focused on investigating MB adsorption through batch experiments. Important thermodynamic parameters can be explored through batch adsorption studies[22,23], while column adsorption studies provide valuable insights into the suitability and scalability of adsorbent utilization[24]. Breakthrough analysis can be used to explore the dynamics and characteristics of column adsorption[25].

In this study, we evaluated the potential of utilizing commercial biochar for MB removal in a continuous adsorption mode. We examined the effects of pH, inflow rate (Q), bed height (Z), and inlet MB concentration (C_0) on MB adsorption. To understand the theoretical basis of MB adsorption, we employed and analyzed the Thomas, Bohart-Adams, Yoon-Nelson, and Bed Depth Service Time (BDST) models. Furthermore, we evaluated the contribution of mass transfer and interaction in MB adsorption using the proposed serial exponential-logistic model, demonstrating a good agreement with experimental data.

Experimental

Adsorbent preparation

Commercial biochar derived from melaleuca wood was locally collected from Tien Giang Province, Vietnam. The raw material was milled and sieved to obtain particles ranging in size from 1 to 2 mm. Subsequently, the biochar particles were dried at 120 °C for 4 hours. The resulting adsorbent was then stored in a sealed plastic bag.

Instrumentation

The specific surface area and pore size distribution of the biochar were determined by analyzing nitrogen adsorption and desorption isotherms using Surfer equipment (Thermo Scientific Ltd.). The surface morphology of the biochar was examined by scanning electron microscopy with a Prisma E SEM system. An iS5 Nicolet FTIR spectrometer (Thermo Scientific Ltd.) was utilized to record the FTIR spectrum in the wavenumber range from 500 to 4000 cm^{-1}, using KBr as the beam splitter. The concentration of MB in the solution was measured at 640 nm with an Evolution™ 350 UV-Vis spectrophotometer.

Solution preparation

Analytical-grade methylene blue trihydrate ($C_{16}H_{18}ClN_3S \cdot 3H_2O$) from Xilong (China) was used to prepare the adsorbate solutions. A stock solution of MB was prepared by dissolving 1.169 g of MB in 1.0 L of distilled water, resulting in a concentration of 1000 mg L^{-1}. This stock solution was then diluted to the desired concentration for the continuous adsorption experiments. The initial pH of the MB solutions was adjusted using solutions of HCl (0.1 mol L^{-1}) and NaOH (0.1 mol L^{-1}).

Continuous adsorption studies

Poly(vinyl chloride) pipes with an inner diameter of 21 mm were utilized in this study. These pipes were filled with adsorbent particles, and the bed height varied between 16, 40, and 65 cm. Glass wool layers were employed to secure the adsorbent bed at the bottom and top of the pipes. The MB solution was continuously pumped upward to prevent gravitational effects, which could lead to incomplete saturation of the solution in the adsorption column. The treated stream was discharged at the top of the bed, and collected at regular intervals of 60 seconds. The effects of inflow rate (Q = 5, 10, 15, and 20 mL min^{-1}), pH (3, 4, 6, 7, and 9), bed height (Z = 16, 40, and 65 cm), and inlet MB concentration (C_0 = 0.75, 2.5, 6.5, and 9 mg L^{-1}) on MB adsorption performance were investigated.

Results and discussion

Characterization of the adsorbent

The porous structure of the biochar was investigated through N_2 adsorption-desorption analysis (Fig. 1). As presented in Fig. 1, the volume of adsorbed N_2 rapidly increased at P/P_0 less than 0.2 or higher than 0.7, and reached a plateau in the middle

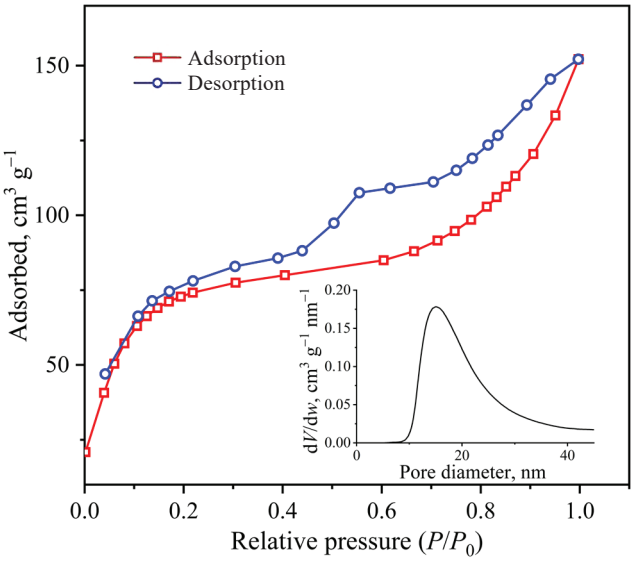

Fig. 1 – *Nitrogen adsorption-desorption isotherm*

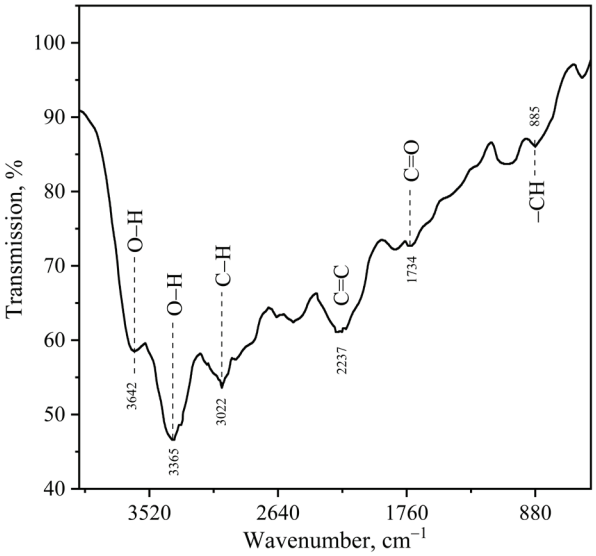

Fig. 2 – *FTIR spectrum of charcoal*

of the range. A hysteresis loop appeared at P/P_0 near 0.4, which depicts capillary condensation in mesopores[26,27]. These findings, along with the pore size distribution (inset in Fig. 1), indicate the presence of micro-, meso-, and macro-pore structures in the adsorbent, with the mesopore structure being predominant. The BET surface area and pore volume were determined to be 274.2 m^2 g^{-1} and 0.44 cm^3 g^{-1}, respectively.

The chemical functional groups on the surface of the biochar were determined using FTIR spectroscopy. The FTIR spectrum (Fig. 2) reveals peaks at 3365 and 3642 cm^{-1}, associated with the O–H bond stretching mode of free water and functional groups on the biochar surface, respectively[28]. The characteristic peak at 3022 cm^{-1} is attributed to C–H stretching vibration. The absorption band at 2237 cm^{-1} corresponds to the C=C bond of aromatic rings within the biochar structure[29]. The appearance of the band at 1734 cm^{-1} corresponds to the C=O stretching vibration[30], while the bending peak at 885 cm^{-1} represents the vibration of the aromatic –CH group[31]. The unsaturated C=C and C=O groups can be deprotonated, thereby enhancing the interaction between the biochar and the cationic dye MB[32]. This FTIR analysis confirms the presence of functional groups on the biochar surface, consistent with previous reports for other biochars[28,31,33].

SEM images at 160× and 1200× magnification (Fig. 3) reveal the porous structure of the biochar. The biochar exhibits interconnected trenches and tunnels of varying diameters, forming a matrix with open channels. This structure facilitates the penetration of MB into the inner surface of the biochar[34]. However, the heterogeneity in size and shape of these trenches and tunnels may impede the diffusion of MB molecules within the biochar, resulting in a slow rate of MB adsorption[35].

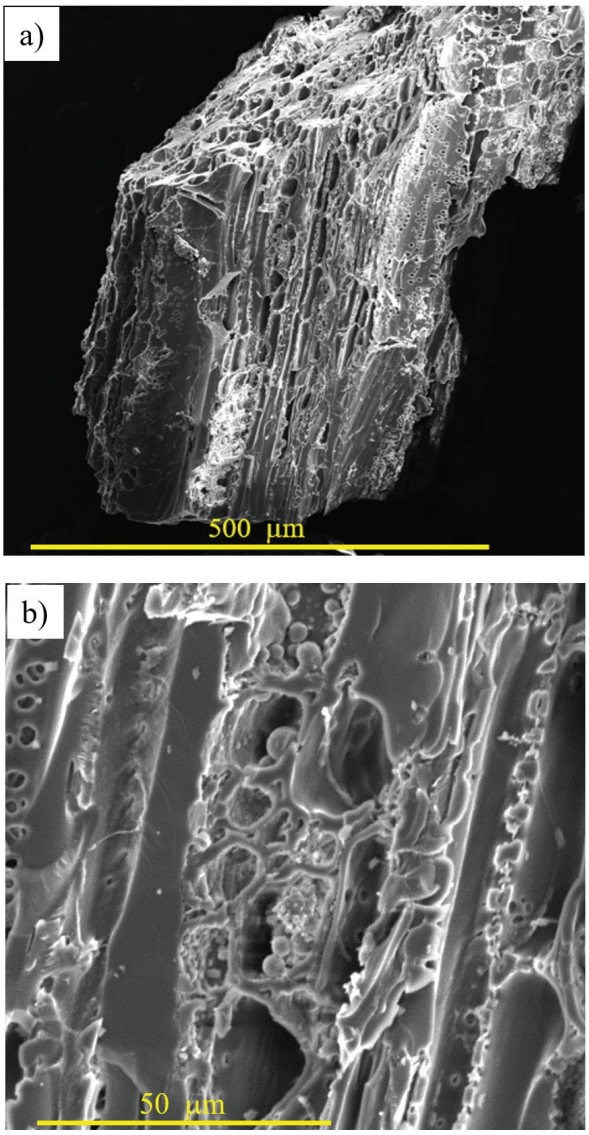

Fig. 3 – *SEM images of charcoal at a) 160×, and b) 1200× magnification*

Effects of operating parameters on adsorption

Column adsorption studies play a significant role in assessing the practical applicability of adsorbents in industrial settings. The effects of the initial pH, inflow rate, bed height, and inlet MB concentration on MB removal were investigated in the continuous adsorption mode. The obtained breakthrough curves (BTCs) are depicted by the discrete points in Fig. 4. Overall, the characteristic S-shape of the BTCs was not clearly discernible.

Effect of pH

The pH variations affect the formation and activation of functional groups on the biochar surface, thereby influencing the surface charge. As pH value increases, the unsaturated C=C and C=O groups undergo deprotonation, resulting in a more negative surface charge. This result promotes electrostatic interactions between the cationic dye MB and the biochar surface[32], leading to accelerated MB adsorption.

Fig. 4a displays the experimental BTCs at various pH values. With increasing pH values, MB adsorption reached saturation ($C/C_0 \rightarrow 1$) more rapidly. The BTCs at different pH values exhibited a notable trend where MB breakthrough occurred instantaneously as the MB solution was plugged.

Effect of inflow rate

Fig. 4b presents the adsorption performance of MB at different inflow rates. At low inflow rates (5 mL min^{-1}), the residence time of MB in the adsorbent bed was prolonged, facilitating the intra-particle phenomenon, where MB diffuses into the inner

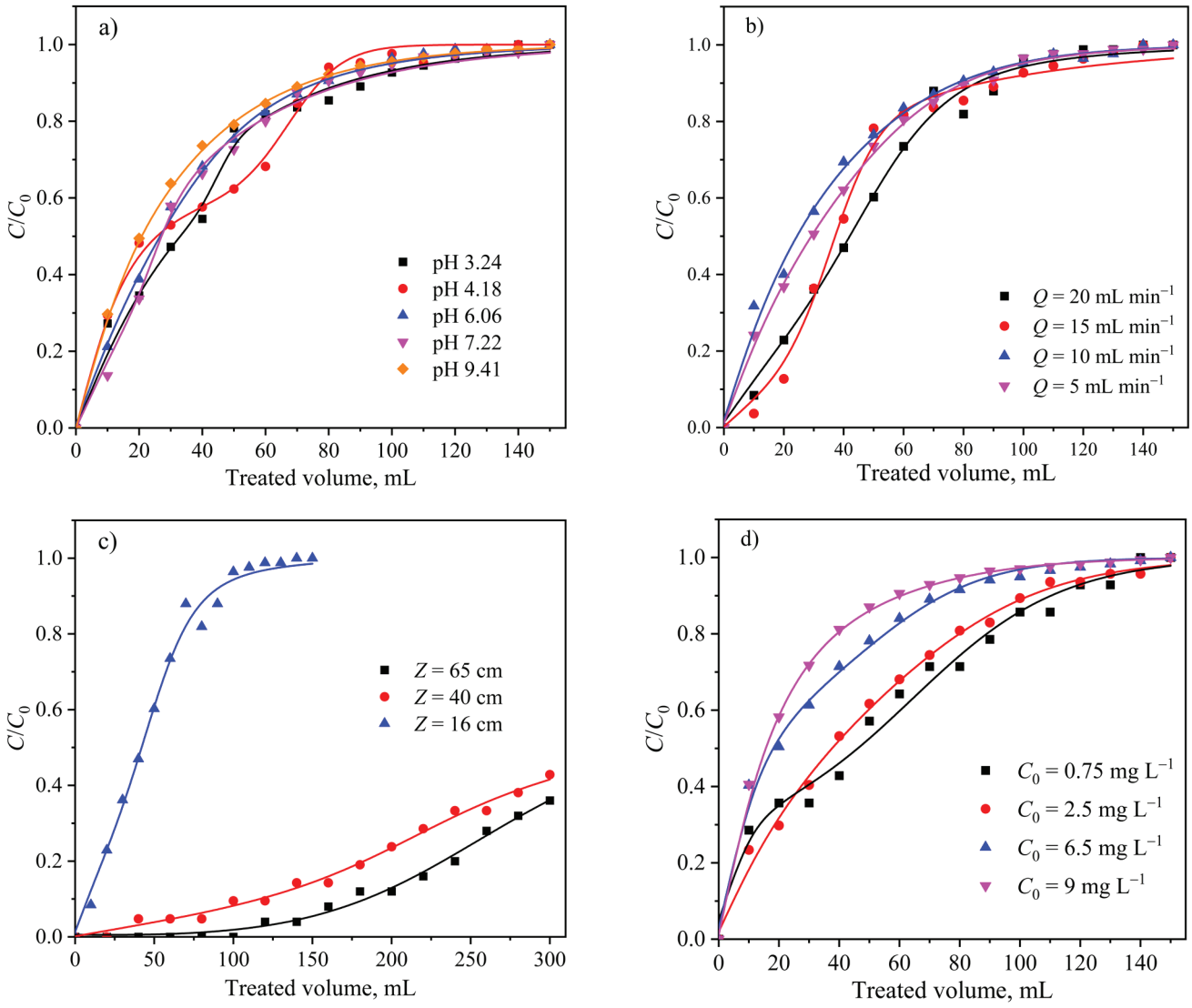

Fig. 4 – *Influence of a) initial pH (Q = 10 mL min^{-1}, Z = 16 cm, C_0 = 5 mg L^{-1}), b) inflow rate (pH 7.5, Z = 16 cm, C_0 = 5 mg L^{-1}), c) bed height (pH 7.5, Q = 10 mL min^{-1}, C_0 = 5 mg L^{-1}), and d) inlet MB concentration (pH 6.5, Q = 10 mL min^{-1}, Z = 16 cm) on breakthrough curves*

surface of the biochar's porous structure[36]. This suggested enhanced penetration of MB molecules into the biochar, increasing adsorption opportunities. Conversely, at higher inflow rates, MB primarily adsorbed onto the external surface of the biochar, resulting in steeper BTCs[37]. As shown in Fig. 4b, the BTC obtained at an inflow rate of 5 mL min^{-1} displays an S-shaped curve, indicating that mass transfer and internal resistance governed adsorption performance of MB[38].

Effect of adsorbent bed height

The adsorption of MB was performed at different adsorbent bed heights, revealing the BTCs as shown in Fig. 4c. The BTCs obtained at bed heights of 40 and 65 cm exhibited similar shapes but differed significantly from the 16 cm bed height BTC. Increasing bed height led to a longer breakthrough time, indicating enhanced MB adsorption capacity of the biochar. This was because a greater mass of the biochar was used, providing more adsorptive sites[38,39]. Moreover, as the bed height increased, the tortuosity of the transfer pathways for MB through the biochar bed also increased, promoting collisions between MB molecules and the adsorption sites[40]. Consequently, the BTC obtained at a higher bed height displayed a gentler slope and a longer breakthrough time, as shown in Fig. 4c.

Effect of inlet MB concentration

Fig. 4d presents the BCTs of MB adsorption with varying C_0 values (0.75, 2.5, 6.5, and 9 mg L^{-1}). The BTCs exhibit a steeper slope with an increased C_0, indicating a faster MB breakthrough. As the C_0 increases, the probability of collision between MB molecules and adsorption sites increases, leading to a decrease in the time required to reach saturation[40].

Breakthrough curve analysis

Thomas model

The Thomas model (Eq. (1)) has been widely used to predict BTCs by considering the adsorption-desorption isotherm of Langmuir kinetics and ignoring the resistances of external and internal diffusion[41]. If column adsorption data follows the Thomas model, the adsorption processes predominantly occur at the external surface of the adsorbent rather than being governed by a chemical process[42,43]. Non-linear fits of experimental results to the Thomas model reveal a considerable correlation ($R^2 > 0.9$), as shown in Table 1. The K_{Th} value, representing the adsorption rate, exhibits minor changes with pH and Q variations, whereas this parameter increases with increasing Z and C_0. This trend is consistent with previous studies[44,45]. Additionally, Russo *et al.*[38] found that an increase in C_0 results in an enhancement in the mass transfer driving force, which subsequently leads to a rise in the K_{Th} constant. The model equation is:

$$\frac{C}{C_0} = \frac{1}{1 + e^{\frac{K_{Th}}{Q}(q_{Th}w - C_0V)}} \tag{1}$$

where C is the MB concentration in the outlet flow (mg L^{-1}), K_{Th} is the Thomas rate constant (L mg^{-1} min^{-1}), q_{Th} is the equilibrium MB adsorption (mg kg^{-1}), w is the weight of the biochar in column (kg), Q is the volumetric flow rate (L min^{-1}), and V is the treated effluent volume (L).

The theoretical maximum adsorption capacity, q_{max} (mg kg^{-1}), can be calculated according to Eq. (2):

$$q_{max} = \frac{C_0}{w}\int_0^{\infty}\left(1 - \frac{C_t}{C_0}\right)dV \tag{2}$$

Applying Eq. (2) to the Thomas model, the Thomas maximum adsorption capacity can be determined by the following algebraic equation:

$$q_{Th,max} = \frac{Q}{wK_{Th}}\ln\left(1 + e^{\frac{K_{Th}q_{Th}w}{Q}}\right) \tag{3}$$

At low pH (3.24), the excess H^+ in solution can protonate functional groups on the biochar surface, resulting in a low $q_{Th,max}$ for MB[46]. At high pH (9.41), the free OH^- can compete with MB for adsorption sites[47], causing a fast saturation of the biochar and resulting in a low $q_{Th,max}$. Notably, the experimental results show that the removal of MB is less affected within the pH range of 4–7. Another important parameter that affects the MB adsorption performance is C_0. With increasing C_0, the driving force, also referred to as the concentration gradient from the solution to the adsorbent surface, intensifies. As a result, more adsorption sites become occupied, leading to a higher value of $q_{Th,max}$[46,48,49].

Over different inflow rates, the calculated $q_{Th,max}$ values remained almost unchanged. This finding demonstrates that the breakthrough time was significantly shorter than the residence time. This is the characteristic difference between the biochar and other adsorbents with large $q_{Th,max}$ values, such as phoenix tree leaf powder ($q_{Th,max}$ = 135 mg g^{-1})[48], palm shell-based activated carbon ($q_{Th,max}$ = 115.87 mg g^{-1})[50], groundnut shell powder ($q_{Th,max}$ = 272 mg g^{-1})[51].

The effect of Z on the $q_{Th,max}$ is also displayed in Table 1. The results revealed a decrease in $q_{Th,max}$ as Z increased, contrary to previous reports[49,52]. However, it should be noted that Kumar *et al.*[51] found no definitive effect of bed height on $q_{Th,max}$.

Table 1 – *Thomas parameters obtained*

pH	Q, mL min^{-1}	Z, cm	C_0, mg L^{-1}	K_{Th}, L mg^{-1} min^{-1}	q_{Th}, mg kg^{-1}	R^2	$q_{Th,max}$, mg kg^{-1}
3.24	10	16	5	0.17	10.7	0.9677	11.8
4.18	10	16	5	0.10	16.1	0.9483	18.3
6.06	10	16	5	0.14	14.6	0.9745	15.7
7.22	10	16	5	0.12	17.6	0.9699	18.8
9.41	10	16	5	0.13	13.1	0.9582	14.7
7.5	5	16	5	0.26	12.3	0.9734	12.3
7.5	10	16	5	0.13	20.4	0.9230	21.1
7.5	15	16	5	0.12	16.3	0.9790	19.8
7.5	20	16	5	0.13	13.9	0.9672	19.9
7.5	10	40	5	0.10	15.4	0.9766	15.5
7.5	10	65	5	0.14	9.3	0.9818	9.3
6.5	10	16	0.75	0.46	3.7	0.9629	4.1
6.5	10	16	2.5	0.16	11.3	0.9761	12.5
6.5	10	16	6.5	0.09	16.7	0.9437	19.4
6.5	10	16	9	0.09	18.7	0.9496	21.0

Bohart-Adams model

The Bohart-Adams model (Eq. (4)) assumes that the adsorption equilibrium does not occur instantaneously, and that the adsorption rate is proportional to both the residue capacity of the adsorbent and the concentration of the adsorbate[53]. The adsorption process is controlled by external mass transfer, which is represented by the K_{BA} constant in this model[45,54]. To account for non-equilibrium, the Bohart-Adams model is commonly used to predict the initial portion of BTCs, typically for $C/C_0 < 0.5$ [55].

To determine the parameters of the Bohart-Adams model, the experimental BTCs with $C/C_0 < 0.5$ were fitted using a non-linear approach, and the results are presented in Table 2. The value of K_{BA} varied in a narrow range from 0.009 to 0.016 L mg^{-1} min^{-1} as pH, Q, and C_0 increased. However, as Z increased, this parameter exhibited a significant increase. This result highlighted the dominant role of bed height in influencing the dynamics of MB adsorption through mass transfer. The model equation is:

$$\frac{C}{C_0} = e^{\frac{K_{BA}C_0}{Q}V - K_{BA}N_0\frac{Z}{u}} \quad (4)$$

where K_{BA} is the Bohart-Adams kinetic constant (L mg^{-1} min^{-1}), N_0 is the saturation concentration (mg L^{-1}), Z is the bed height (cm), u is the flow rate (cm min^{-1}).

However, the experimental data did not correlate well with the Bohart-Adams model, as indicated by the low R^2-values presented in Table 2. This suggested that the adsorption equilibrium of MB on the biochar occurred with $C/C_0 < 0.5$.

Yoon-Nelson model

The Yoon-Nelson model (Eq. (5))[56] was applied to analyze the adsorption of MB, assuming that the rate of MB adsorption is proportional to the probability of both MB adsorption and the probability of MB breakthrough on the biochar. The rate constant (K_{YN}) and the time required for 50 % MB breakthrough (τ) were determined and are listed in Table 3 for different conditions. As evident from Table 3, the pH, Q, and Z do not play definitive roles in the variation of the K_{YN}. However, as C_0 increased, the driving force of mass transfer increased, resulting in a more rapid saturation and adsorption rate of the biochar. This led to an increase in K_{YN} and a decrease in τ [48,57]. Furthermore, increased Z resulted in more adsorption sites, enhancing the τ value. This trend was also reported in previous research[48,58]. However, the relationship between τ values and pH, as well as Q, was not clearly established. The model equation is:

$$\frac{C}{C_0} = \frac{e^{K_{YN}\left(\frac{V}{Q}-\tau\right)}}{1+e^{K_{YN}\left(\frac{V}{Q}-\tau\right)}} \quad (5)$$

where K_{YN} is the Yoon-Nelson proportionality constant (min^{-1}), and τ is the time required for removing 50 % of the inlet MB amount (min).

Table 2 – *Bohart-Adams parameters obtained*

pH	Q, mL min^{-1}	Z, cm	C_0, mg L^{-1}	K_{BA}, L mg^{-1} min^{-1}	N_0, mg L^{-1}	R^2
3.24	10	16	5	0.352	4.2	0.8133
4.18	10	16	5	0.299	4.9	0.7620
6.06	10	16	5	0.396	4.5	0.9185
7.22	10	16	5	0.431	4.8	0.9622
9.41	10	16	5	0.534	3.4	0.8780
7.5	5	16	5	0.124	14.2	0.7903
7.5	10	16	5	0.263	7.0	0.9280
7.5	15	16	5	0.339	5.0	0.8652
7.5	20	16	5	0.324	4.8	0.8235
7.5	10	40	5	0.142	4.6	0.9578
7.5	10	65	5	0.178	3.2	0.9696
6.5	10	16	0.75	0.583	1.9	0.8447
6.5	10	16	2.5	0.364	4.1	0.8811
6.5	10	16	6.5	0.328	4.7	0.7381
6.5	10	16	9	–	–	–

Table 3 – *Yoon-Nelson parameters obtained*

pH	Q, mL min^{-1}	Z, cm	C_0, mg L^{-1}	K_{YN}, min^{-1}	τ, min	R^2
3.24	10	16	5	0.52	3.41	0.9677
4.18	10	16	5	0.45	3.31	0.9483
6.06	10	16	5	0.61	3.01	0.9745
7.22	10	16	5	0.62	3.23	0.9699
9.41	10	16	5	0.63	2.52	0.9582
7.5	5	16	5	0.76	3.93	0.9734
7.5	10	16	5	0.58	4.30	0.9879
7.5	15	16	5	0.55	3.28	0.9790
7.5	20	16	5	0.57	2.87	0.9672
7.5	10	40	5	0.21	16.0	0.9766
7.5	10	65	5	0.30	16.7	0.9818
6.5	10	16	0.75	0.34	4.66	0.9629
6.5	10	16	2.5	0.41	4.22	0.9761
6.5	10	16	6.5	0.55	2.46	0.9437
6.5	10	16	9	0.80	1.93	0.9496

Bed depth service time (BDST) model

The BDST model describes the relationship between bed depth (Z) and service time (t), expressed by Eq. (6). This model can be rearranged to show the non-linear relationship between C/C_0 and the volume treated (V), as obeyed in Eq. (7). The BDST model is based on the assumption that the adsorption process is primarily controlled by the surface reaction between the adsorbate and the remaining capacity of the adsorbent[52,54]. The model equations are:

$$t = \frac{N_o}{C_0 u} Z - \frac{1}{K_o C_0} \ln\left(\frac{C_0}{C} - 1\right) \quad (6)$$

$$\frac{C}{C_0} = \frac{1}{1 + e^{\frac{K_o N_o}{u} Z - \frac{K_o C_0}{Q} V}} \quad (7)$$

Table 4 – *BDST parameters obtained*

pH	Q, mL min^{-1}	Z, cm	C_0, mg L^{-1}	K_o, L mg^{-1} min^{-1}	N_o, mg L^{-1}	R^2
3.24	10	16	5	0.104	3.06	0.9677
4.18	10	16	5	0.091	2.97	0.9483
6.06	10	16	5	0.122	2.70	0.9745
7.22	10	16	5	0.124	2.90	0.9699
9.41	10	16	5	0.126	2.26	0.9582
7.5	5	16	5	0.077	3.53	0.9734
7.5	10	16	5	0.116	3.86	0.9879
7.5	15	16	5	0.165	2.94	0.9790
7.5	20	16	5	0.228	2.57	0.9672
7.5	10	40	5	0.022	11.50	0.9766
7.5	10	65	5	0.030	7.36	0.9818
6.5	10	16	0.75	0.457	0.63	0.9629
6.5	10	16	2.5	0.164	1.89	0.9761
6.5	10	16	6.5	0.085	2.86	0.9437
6.5	10	16	9	0.090	3.11	0.9496

where K_o is the adsorption rate constant (L mg^{-1} min^{-1}), N_o is the adsorption capacity (mg L^{-1}).

Non-linear fitting of the BDST model to experimental data yielded the dynamic parameters of the MB adsorption, as presented in Table 4. Theoretically, a lower K_o value indicates a slower mass transfer, necessitating a longer bed depth to prevent breakthrough[59]. As the Q value increased, the mass transfer rate also increased, resulting in a higher K_o value, as shown in Table 4. On the other hand, as C_0 values increased, K_o values decreased, contrasting with the behavior of adsorption capacity (N_o). This trend was also observed by Yagub *et al.*[60] From Table 4, the K_o values are in a low range, indicating that the mass transfer of MB from the fluid phase to the adsorbent surface is a rate-limiting step in the adsorption process. The dependence of K_o and N_o on other conditions was not as regular.

Proposed model of the breakthrough curve of methylene blue adsorption on biochar

The experimental BTCs of MB on biochar, as depicted in Fig. 4, did not exhibit a sharp S-shape due to short breakthrough times. Additionally, several BTCs displayed an intermediate plateau region, such as at pH 4.18 in Fig. 4a, and C_0 = 0.75 mg L^{-1} in Fig. 4d. This suggests that the BTCs for MB adsorption on biochar can be characterized by a serial exponential-logistic pattern. Similar behavior in BTCs has been observed in previous studies on dye adsorption, such as Direct Blue 71 on chitosan-glutaraldehyde biosorbent[52], dye AB25 on commercial activated carbon[61], methyl green on Mobil Composition Matter No. 41 [62], or MB on the tartaric acid-treated bagasse[63]. However, no explanation or mention of this observation has been provided. It notes that the influence of mass transfer on the adsorption rate differs in the initial and final portions[64]. Ghorbanian *et al.*[25] found that the adsorption rate could be governed by either mass diffusion or surface interaction, resulting in a weak satisfactory agreement of the Bohart-Adams and Yoon-Nelson models with the unusual S-shape BTCs.

The biochar initially exhibits a high adsorption capacity due to the abundance of available adsorption sites where MB molecules to bind. Consequently, the rate of MB adsorption is governed by the mass transfer of MB from the external or internal spaces of the biochar particles to the adsorption sites, driven by a concentration gradient. Thus, the initial portion of the BTCs can be described using a logistic function $1/[1+\exp(A–k_1V)]$ [65].

As the total treated volume increases, the residual adsorption capacity of the biochar decreases to a limit. At this point, the rate of adsorption is equivalent to the rate of mass transfer. Beyond this limit, the MB adsorption rate depends on the interaction rate between MB molecules and the unoccupied adsorption sites[66]. This second portion of the BTCs can be characterized as an exponential function $[1–\exp(–k_2V)]$ [67].

The mixing rule[68] was applied to account for the contributions of both mass transfer and interaction to the adsorption performance of MB, resulting

in Eq. (8), which was referred to as the serial logistic-exponential model:

$$\frac{C}{C_0} = \alpha \frac{1}{1+e^{A-k_1V}} + (1-\alpha)\left(1-e^{-k_2V}\right) \qquad (8)$$

where α represents the contribution fraction of the mass transfer; hence, $(1-\alpha)$ indexes the contribution fraction of the interaction.

Clearly, $0 \le \alpha \le 1$. When α is close to 1, the adsorption of MB is primarily controlled by mass transfer. Conversely, when α is close to 0, the adsorption of MB is mainly influenced by interaction. By conducting non-linear fitting with experimental data, four parameters in Eq. (8) were found, and are listed in Table 5. The predicted BTCs following Eq. (8) are illustrated by smooth lines in Fig. 4.

Equation (8) effectively describes the experimental data, as indicated by high R^2-values (>0.998). As presented in Table 5, the values of α were in the medium range (from 0.1 to 0.6), suggesting that the adsorption rate of MB on the biochar cannot be described by the mechanism of mass transfer control. Most values of $\alpha < 0.5$ denoted that the interaction was a predominant influence on the adsorption of MB on the biochar. Additionally, in almost all cases, the ratio of k_1/k_2 was larger than 1, demonstrating the faster rate of mass transfer compared with interaction.

An increase in the values of Q and C_0 decreased the α-value due to the fast saturation of the biochar, resulting in a short time for the first part of the BTCs. Next, the MB adsorption rapidly changed to the second stage, which was governed by interaction. The value of constant A represents the bias contribution of the mass transfer to the overall rate of MB adsorption. A high A-value results in a low value of $1/[1+\exp(A-k_2V)]$, indicating that mass transfer played a trivial role in MB adsorption. At pH 3.24, the A-value was found to be 184, much higher compared to the others. This may have been due to the prevention of MB molecules from interacting with the protonated biochar surface, as discussed previously.

Conclusion

This study investigated the adsorption properties of commercially available biochar derived from melaleuca wood for MB removal in a continuous adsorption system. This biochar exhibited limited affinity for MB adsorption, resulting in short breakthrough times. Most of the obtained BTCs did not conform to the characteristic S-shape pattern associated with regulated diffusion adsorption. The dynamics of MB adsorption were elucidated, with the results aligning well with the serial logistic-exponential models. Notably, the poor compatibility of experimental data with the BDST model suggests that MB adsorption equilibrium was attained swiftly after initiation. Based on the observed behavior of the BTCs, the study determined that the MB adsorption performance was strongly influenced by the combined effects of mass transfer and interaction. Among these, the mass transfer process controlled the adsorption rate of MB on the biochar. This emphasizes the substantial potential of biochar in organic wastewater treatment through advanced adsorption techniques.

Table 5 – *Breakthrough parameters predicted from serial logistic-exponential model*

pH	Q, mL min^{-1}	Z, cm	C_0, mg L^{-1}	A, [–]	k_1, L^{-1}	k_2, L^{-1}	α, [–]	R^2
3.24	10	16	5	184	4.102	0.026	0.12	0.9932
4.18	10	16	5	8.95	0.133	0.073	0.40	0.9961
6.06	10	16	5	2.98	0.087	0.029	0.16	0.9982
7.22	10	16	5	9.15	0.360	0.024	0.19	0.9957
9.41	10	16	5	4.77	0.566	0.031	0.07	0.9997
7.5	5	16	5	5.45	0.150	0.016	0.60	0.9935
7.5	10	16	5	3.65	0.077	0.023	0.54	0.9929
7.5	15	16	5	2.96	0.061	0.030	0.23	0.9984
7.5	20	16	5	2.18	0.044	0.034	0.18	0.9952
7.5	10	40	5	5.00	0.023	0.001	0.27	0.9914
7.5	10	65	5	5.15	0.020	0.000	0.50	0.9896
6.5	10	16	0.75	2.63	0.041	0.161	0.84	0.9868
6.5	10	16	2.5	2.84	0.042	0.028	0.35	0.9961
6.5	10	16	6.5	2.67	0.053	0.091	0.45	0.9961
6.5	10	16	9	2.40	0.040	0.055	0.13	0.9988

ACKNOWLEDGEMENT

We acknowledge Ho Chi Minh City University of Technology (HCMUT), VNU-HCM for supporting this study.

CONFLICTS OF INTEREST

There is no conflict of interest among the involved institutions.

References

1. *Khan, I., Saeed, K., Zekker, I., Zhang, B., Hendi, A. H., Ahmad, A., Ahmad, S., Zada, N., Ahmad, H., Shah, L. A., Shah, T., Khan, I.,* Review on methylene blue: Its properties, uses, toxicity and photodegradation, Water **14**(2) (2022) 242. doi: https://doi.org/10.3390/w14020242
2. *Oladoye, P. O., Ajiboye, T. O., Omotola, E. O., Oyewola, O. J.,* Methylene blue dye: Toxicity and potential elimination technology from wastewater, Results Eng. **16** (2022) 100678. doi: https://doi.org/10.1016/j.rineng.2022.100678
3. *Ramakrishnan, R. K., Padil, V. V. T., Wacławek, S., Černík, M., Varma, R. S.,* Eco-friendly and economic, adsorptive removal of cationic and anionic dyes by bio-based karaya gum-chitosan sponge, Polymers **13**(2) (2021) 251. doi: https://doi.org/10.3390/polym13020251
4. *Benosmane, N., Boutemeur, B., Hamdi, S. M., Hamdi, M.,* Removal of methylene blue dye from aqueous solutions using polymer inclusion membrane technology, Appl. Water Sci. **12**(5) (2022) 104. doi: https://doi.org/10.1007/s13201-022-01627-1
5. *Cheng, J., Zhan, C., Wu, J., Cui, Z., Si, J., Wang, Q., Peng, X., Turng, L.-S.,* Highly efficient removal of methylene blue dye from an aqueous solution using cellulose acetate nanofibrous membranes modified by polydopamine, ACS Omega **5**(10) (2020) 5389. doi: https://doi.org/10.1021/acsomega.9b04425
6. *Dutta, K., Mukhopadhyay, S., Bhattacharjee, S., Chaudhuri, B.,* Chemical oxidation of methylene blue using a Fenton-like reaction, J. Hazard. Mater. **84**(1) (2001) 57. doi: https://doi.org/10.1016/S0304-3894(01)00202-3
7. *Ibrahim, S. M., Al-Hossainy, A. F., Saha, B., Abd El-Aal, M.,* Removal of bromothymol blue dye by the oxidation method using $KMnO_4$: Accelerating the oxidation reaction by Ru(III) catalyst, J. Mol. Struct. **1268** (2022) 133679. doi: https://doi.org/10.1016/j.molstruc.2022.133679
8. *Contreras, M., Grande-Tovar, C. D., Vallejo, W., Chaves-López, C.,* Bio-removal of methylene blue from aqueous solution by *Galactomyces geotrichum* KL20A, Water **11**(2) (2019) 282. doi: https://doi.org/10.3390/w11020282
9. *Wu, K., Shi, M., Pan, X., Zhang, J., Zhang, X., Shen, T., Tian, Y.,* Decolourization and biodegradation of methylene blue dye by a ligninolytic enzyme-producing *Bacillus thuringiensis*: Degradation products and pathway, Enzyme Microb. Technol. **156** (2022) 109999. doi: https://doi.org/10.1016/j.enzmictec.2022.109999
10. *Slimani, R., Ouahabi, I. E., Benkaddour, S., Hiyane, H., Essoufy, M., Achour, Y., Antri, S. E., Lazar, S., Haddad, M. E.,* Removal efficiency of textile dyes from aqueous solutions using calcined waste of eggshells as eco-friendly adsorbent: Kinetic and thermodynamic studies, Chem. Biochem. Eng. Q. **35**(1) (2021) 43. doi: https://doi.org/10.15255/CABEQ.2020.1872
11. *Ilgin, P., Onder, A., Kıvanç, M. R., Ozay, H., Ozay, O.,* Adsorption of methylene blue from aqueous solution using poly (2-acrylamido-2-methyl-1-propanesulfonic acid-co-2-hydroxyethyl methacrylate) hydrogel crosslinked by activated carbon, J. Macromol. Sci., A **60**(2) (2023) 135. doi: https://doi.org/10.1080/10601325.2023.2165945
12. *Fito, J., Abewaa, M., Mengistu, A., Angassa, K., Ambaye, A. D., Moyo, W., Nkambule, T.,* Adsorption of methylene blue from textile industrial wastewater using activated carbon developed from *Rumex abyssinicus* plant, Sci. Rep. **13**(1) (2023) 5427. doi: https://doi.org/10.1038/s41598-023-32341-w
13. *Al-Ghouti, M. A., Al-Absi, R. S.,* Mechanistic understanding of the adsorption and thermodynamic aspects of cationic methylene blue dye onto cellulosic olive stones biomass from wastewater, Sci. Rep. **10**(1) (2020) 15928. doi: https://doi.org/10.1038/s41598-020-72996-3
14. *El-Bery, H. M., Saleh, M., El-Gendy, R. A., Saleh, M. R., Thabet, S. M.,* High adsorption capacity of phenol and methylene blue using activated carbon derived from lignocellulosic agriculture wastes, Sci. Rep. **12**(1) (2022) 5499. doi: https://doi.org/10.1038/s41598-022-09475-4
15. *Ying, Z., Chen, X., Li, H., Liu, X., Zhang, C., Zhang, J., Yi, G.,* Efficient adsorption of methylene blue by porous biochar derived from soybean dreg using a one-pot synthesis method, Molecules **26**(3) (2021) 661. doi: https://doi.org/10.3390/molecules26030661
16. *Bui, H. T., Le, T. P., Nguyen, T. P., Le, D. N., Vo, D. L., Pham, L. A., Nguyen, L. L., Nguyen, T. H., Le, T. V., Huong, M., Dinh, T. M. T., Herrmann, M., Ouillon, S., Duong, T. T., Le, T. P. Q.,* Removal of methylene blue from aqueous solution by biochar derived from rice husk, Vietnam J. Earth Sci. **44**(2) (2022) 273. doi: https://doi.org/10.15625/2615-9783/16998
17. *Banerjee, S., Chattopadhyaya, M. C., Srivastava, V., Sharma, Y. C.,* Adsorption studies of methylene blue onto activated saw dust: Kinetics, equilibrium, and thermodynamic studies, Environ. Prog. Sustain. Energy **33**(3) (2014) 790. doi: https://doi.org/10.1002/ep.11840
18. *Shih, M.-C.,* Kinetics of the batch adsorption of methylene blue from aqueous solutions onto rice husk: Effect of acid-modified process and dye concentration, Desalin. Water Treat. **37**(1-3) (2012) 200. doi: https://doi.org/10.1080/19443994.2012.661273
19. *Lonappan, L., Rouissi, T., Das, R. K., Brar, S. K., Ramirez, A. A., Verma, M., Surampalli, R. Y., Valero, J. R.,* Adsorption of methylene blue on biochar microparticles derived from different waste materials, Waste Manage. **49** (2016) 537. doi: https://doi.org/10.1016/j.wasman.2016.01.015
20. *Sahu, S., Pahi, S., Tripathy, S., Singh, S. K., Behera, A., Sahu, U. K., Patel, R. K.,* Adsorption of methylene blue on chemically modified lychee seed biochar: Dynamic, equilibrium, and thermodynamic study, J. Mol. Liq. **315** (2020) 113743. doi: https://doi.org/10.1016/j.molliq.2020.113743
21. *Hassaan, M. A., Yılmaz, M., Helal, M., El-Nemr, M. A., Ragab, S., El Nemr, A.,* Improved methylene blue adsorption from an aqueous medium by ozone-triethylenetetramine modification of sawdust-based biochar, Sci. Rep. **13** (2023) 12431. doi: https://doi.org/10.1038/s41598-023-39495-7

22. *Bouabdallah, A. B., Mazari, F., Sifi, R.,* Removal of solophenyl red 3BL dye from textile effluents by adsorption using a natural adsorbent *Oxalis pes-caprae* L., Chem. Biochem. Eng. Q. **37**(1) (2023) 45. doi: https://doi.org/10.15255/CABEQ.2022.2165
23. *Dim, P. E., Termtanun, M.,* Treated clay mineral as adsorbent for the removal of heavy metals from aqueous solution, Appl. Sci. Eng. Prog. **14**(3) (2021) 511. doi: http://doi.org/10.14416/j.asep.2021.04.002
24. *Sazali, N., Harun, Z., Sazali, N.,* A review on batch and column adsorption of various adsorbent towards the removal of heavy metal, J. Adv. Res. Fluid Mech. Therm. Sci. **67**(2) (2020) 66.
25. *Ghorbanian, S., Davoudinejad, M., Khakpay, A., Radpour, S.,* Investigation of breakthrough curves of citric acid adsorption, Chem. Biochem. Eng. Q. **28**(3) (2014) 329. doi: https://doi.org/10.15255/CABEQ.2013.1872
26. *Patel, H.,* Fixed-bed column adsorption study: A comprehensive review, Appl. Water Sci. **9** (2019) 45. doi: https://doi.org/10.1007/s13201-019-0927-7
27. *Fang, K., Yang, R.,* A comparison on the efficiency of raw activated carbon, oxidized, and sulfurized adsorbents for furfural adsorption, Alex. Eng. J. **60**(1) (2021) 1241. doi: https://doi.org/10.1016/j.aej.2020.10.047
28. *Jun-Jie, G., Ye-Bo, Q., Tao, Z., Dong-Dong, C., Ping, X., Danielle, H., Yue-Fei, W.,* Adsorption of methylene blue onto activated carbon produced from tea (*Camellia sinensis* L.) seed shells: Kinetics, equilibrium, and thermodynamics studies, J. Zhejiang Univ. Sci. B **14** (2013) 650. doi: https://doi.org/10.1631/jzus.B12a0225
29. *Adeniyi, A. G., Ighalo, J. O., Onifade, D. V.,* Production of biochar from elephant grass (*Pernisetum purpureum*) using an updraft biomass gasifier with retort heating, Biofuels **12**(10) (2019) 1283. doi: https://doi.org/10.1080/17597269.2019.1613751
30. *Bashyal, N., Aryal, S., Rai, R., Lohani, P., Gautam, S., Pokhrel, M., Poudel, B.,* Effective biosorption of phosphate from water using Fe(III)-loaded pomegranate peel, Chem. Biochem. Eng. Q. **37**(2) (2023) 67. doi: https://doi.org/10.15255/CABEQ.2022.2174
31. *Liu, X., Liao, J., Song, H., Yang, Y., Guan, C., Zhang, Z.,* A biochar-based route for environmentally friendly controlled release of nitrogen: Urea-loaded biochar and bentonite composite, Sci. Rep. **9** (2019) 9548. doi: https://doi.org/10.1038/s41598-019-46065-3
32. *Zhang, K., Sun, P., Zhang, Y.,* Decontamination of Cr(VI) facilitated formation of persistent free radicals on rice husk derived biochar, Front. Environ. Sci. Eng. **13** (2019) 22. doi: https://doi.org/10.1007/s11783-019-1106-7
33. *Liu, S., Peng, S., Zhang, B., Xue, B., Yang, Z., Wang, S., Xu, G.,* Effects of biochar pyrolysis temperature on thermal properties of polyethylene glycol/biochar composites as shape-stable biocomposite phase change materials, RSC Adv. **12**(16) (2022) 9587. doi: https://doi.org/10.1039/D1RA09167K
34. *Yong, Y., Lou, X., Li, S., Yang, C., Yin, X.,* Direct simulation of the influence of the pore structure on the diffusion process in porous media, Comput. Math. Appl. **67**(2) (2014) 412. doi: https://doi.org/10.1016/j.camwa.2013.08.032
35. *Cai, Y., Liu, L., Tian, H., Yang, Z., Luo, X.,* Adsorption and desorption performance and mechanism of tetracycline hydrochloride by activated carbon-based adsorbents derived from sugar cane bagasse activated with $ZnCl_2$, Molecules **24**(24) (2019) 4534. doi: https://doi.org/10.3390/molecules24244534
36. *Suwannatrai, S., Yan, D. Y., Khamdahsag, P., Tanboonchuy, V.,* Zeolite/cerium oxide coat-on activated alumina ball for arsenite removal via fixed-bed continuous flow adsorption column, Appl. Sci. Eng. Prog. **15**(4) (2022) No. 5571. doi: https://doi.org/10.14416/j.asep.2021.11.004
37. *Chen, C., Chen, Z., Shen, J., Kang, J., Zhao, S., Wang, B., Chen, Q., Li, X.,* Dynamic adsorption models and artificial neural network prediction of mercury adsorption by a dendrimer-grafted polyacrylonitrile fiber in fixed-bed column, J. Clean. Prod. **310** (2021) 127511. doi: https://doi.org/10.1016/j.jclepro.2021.127511
38. *Russo, V., Masiello, D., Trifuoggi, M., Serio, M. D., Tesser, R.,* Design of an adsorption column for methylene blue abatement over silica: From batch to continuous modeling, Chem. Eng. J. **302** (2016) 287. doi: https://doi.org/10.1016/j.cej.2016.05.020
39. *Bakka, A., Mamouni, R., Saffaj, N., Laknifli, A., Aziz, K., Roudani, A.,* Removal of bifenthrin pesticide from aqueous solutions by treated patellidae shells using a new fixed bed column filtration technique, Process Saf. Environ. Prot. **143** (2020) 55. doi: https://doi.org/10.1016/j.psep.2020.06.030
40. *Muñoz-Cobo, J.-L., Berna, C.,* Chemical kinetics roots and methods to obtain the probability distribution function evolution of reactants and products in chemical networks governed by a master equation, Entropy **21**(2) (2019) 181. doi: https://doi.org/10.3390/e21020181
41. *Thomas, H. C.,* Heterogeneous ion exchange in a flowing system, J. Am. Chem. Soc. **66**(10) (1944) 1664. doi: https://doi.org/10.1021/ja01238a017
42. *Solgi, M., Tabil, L. G., Wilson, L. D.,* Modified biopolymer adsorbents for column treatment of sulfate species in saline aquifers, Materials **13**(10) (2020) 2408. doi: https://doi.org/10.3390/ma13102408
43. *Hasan, S. H., Ranjan, D., Talat, M.,* Agro-industrial waste 'wheat bran' for the biosorptive remediation of selenium through continuous up-flow fixed-bed column, J. Hazard. Mater. **181**(1-3) (2010) 1134. doi: https://doi.org/10.1016/j.jhazmat.2010.05.133
44. *Patel, H., Vashi, R. T.,* Fixed bed column adsorption of ACID Yellow 17 dye onto Tamarind seed powder, Can. J. Chem. Eng. **90**(1) (2012) 180. doi: https://doi.org/10.1002/cjce.20518
45. *Lakshmipathy, R., Sarada, N. C.,* Methylene blue adsorption onto native watermelon rind: Batch and fixed bed column studies, Desalin. Water Treat. **57**(23) (2016) 10632. doi: https://doi.org/10.1080/19443994.2015.1040462
46. *Amode, J. O., Santos, J. H., Md. Alam, Z., Mirza, A. H., Mei, C. C.,* Adsorption of methylene blue from aqueous solution using untreated and treated (*Metroxylon* spp.) waste adsorbent: Equilibrium and kinetics studies, Int. J. Ind. Chem. **7** (2016) 333. doi: https://doi.org/10.1007/s40090-016-0085-9
47. *Saputra, E., Saputra, R., Nugraha, M. W., Irianty, R. S., Utama, P. S.*, Removal of Methylene Blue from aqueous solution using spent bleaching earth, in: 2nd International Conference on Oleo and Petrochemical Engineering (ICOOPChE 2017), Pekanbaru-Riau, Indonesia (2017) 012008. doi: https://doi.org/10.1088/1757-899X/345/1/012008
48. *Han, R., Wang, Y., Zhao, X., Wang, Y., Xie, F., Cheng, J., Tang, M.,* Adsorption of methylene blue by phoenix tree leaf powder in a fixed-bed column: Experiments and prediction of breakthrough curves, Desalination **245**(1-3) (2009) 284. doi: https://doi.org/10.1016/j.desal.2008.07.013

49. *Gong, J.-L., Zhang, Y.-L., Jiang, Y., Zeng, G.-M., Cui, Z.-H., Liu, K., Deng, C.-H., Niu, Q.-Y., Deng, J.-H., Huan, S.-Y.,* Continuous adsorption of Pb(II) and methylene blue by engineered graphite oxide coated sand in fixed-bed column, Appl. Surf. Sci. **330** (2015) 148.
doi: https://doi.org/10.1016/j.apsusc.2014.11.068
50. *Khasri, A., Azmi, N. A. F., Jamir, M. R. M., Ahmad, M. A.*, Continuous fixed bed adsorption of methylene blue onto microwave-assisted palm shell based activated carbon, in: International Conference on Trends in Chemical Engineering 2021 (ICoTRiCE2021), University Malaysia Perlis, Pauh, Perlis (2022) 040006.
doi: https://doi.org/10.1063/5.0113753
51. *Kumar, S., Gunasekar, V., Ponnusami, V.,* Removal of methylene blue from aqueous effluent using fixed bed of groundnut shell powder, J. Chem. **2013** (2013) ID 259819.
doi: https://doi.org/10.1155/2013/259819
52. *López-Cervantes, J., Sánchez-Machado, D. I., Sánchez-Duarte, R. G., Correa-Murrieta, M. A.,* Study of a fixed-bed column in the adsorption of an azo dye from an aqueous medium using a chitosan-glutaraldehyde biosorbent, Adsorpt. Sci. Technol. **36**(1-2) (2018) 215.
doi: https://doi.org/10.1177/0263617416688
53. *Bohart, G. S., Adams, E. Q.,* Some aspects of the behavior of charcoal with respect to chlorine, J. Am. Chem. Soc. **42**(3) (1920) 523.
doi: https://doi.org/10.1021/ja01448a018
54. *Ostaszewski, P., Długosz, O., Banach, M.,* Analysis of measuring methods of the concentration of methylene blue in the sorption process in fixed-bed column, Int. J. Environ. Sci. Technol. **19** (2022) 1.
doi: https://doi.org/10.1007/s13762-021-03156-x
55. *Hu, Q., Pang, S., Wang, D., Yang, Y., Liu, H.,* Deeper insights into the Bohart–Adams model in a fixed-bed column, J. Phys. Chem. B **125**(30) (2021) 8494.
doi: https://doi.org/10.1021/acs.jpcb.1c03378
56. *Yoon, Y. H., Nelson, J. H.,* Application of gas adsorption kinetics I. A theoretical model for respirator cartridge service life, Am. Ind. Hyg. Assoc. J. **45**(8) (1984) 509.
doi: https://doi.org/10.1080/15298668491400197
57. *Afroze, S., Sen, T. K., Ang, H. M.,* Adsorption performance of continuous fixed bed column for the removal of methylene blue (MB) dye using *Eucalyptus sheathiana* bark biomass, Res. Chem. Intermed. **42** (2016) 2343.
doi: https://doi.org/10.1007/s11164-015-2153-8
58. *Lissy, P. N. M., Madhu, G., Thomas, R. M.,* Modeling of packed bed column studies for the removal of Cu(II) using polypyrrole alumina iron oxide nanocomposite, Desalin. Water Treat. **227** (2021) 278.
doi: https://doi.org/10.5004/dwt.2021.27293
59. *JagadeeshBabu, P. E., Krishnan, R., Singh, M.,* Bed depth service time model for the biosorption of reactive red dye using the *Portunus sanguinolentus* shell, Asia-Pac. J. Chem. Eng. **5**(5) (2009) 791.
doi: https://doi.org/10.1002/apj.408
60. *Yagub, M. T., Sen, T. K., Afroze, S., Ang, H. M.,* Fixed-bed dynamic column adsorption study of methylene blue (MB) onto pine cone, Desalin. Water Treat. **55**(4) (2015) 1026.
doi: https://doi.org/10.1080/19443994.2014.924034
61. *Hernandez-Eudave, M. T., Bonilla-Petriciolet, A., Moreno-Virgen, M. R., Rojas-Mayorga, C. K., Tovar-Gómez, R.,* Design analysis of fixed-bed synergic adsorption of heavy metals and acid blue 25 on activated carbon, Desalin. Water Treat. **57**(21) (2016) 9824.
doi: https://doi.org/10.1080/19443994.2015.1031710
62. *Alardhi, S. M., Albayati, T. M., Alrubaye, J. M.,* Adsorption of the methyl green dye pollutant from aqueous solution using mesoporous materials MCM-41 in a fixed-bed column, Heliyon **6**(1) (2020) e03253.
doi: https://doi.org/10.1016/j.heliyon.2020.e03253
63. *Low, L. W., Teng, T. T., Morad, N., Azahari, B.,* Optimization of the column studies into the adsorption of basic dye using tartaric acid-treated bagasse, Desalin. Water Treat. **52**(31-33) (2014) 6194.
doi: https://doi.org/10.1080/19443994.2013.817630
64. *Malina, J., Rađenović, A.,* Kinetic aspects of methylene blue adsorption on blast furnace sludge, Chem. Biochem. Eng. Q. **28**(4) (2014) 491.
doi: https://doi.org/10.15255/CABEQ.2014.19366
65. *Clark, R. M.,* Modeling TOC removal by GAC: The general logistic function, J. Am. Water Works Assoc. **79**(1) (1987) 33.
doi: https://doi.org/10.1002/j.1551-8833.1987.tb02780.x
66. *Kónya, J., Nagy, N. M.,* Isotherm equation of sorption of electrolyte solutions on solids: How to do heterogeneous surface from homogeneous one ?, Period. Polytech. Chem. Eng. **53**(2) (2009) 55.
doi: https://doi.org/10.3311/pp.ch.2009-2.04
67. *Hu, Q., Xie, Y., Feng, C., Zhang, Z.,* Prediction of breakthrough behaviors using logistic, hyperbolic tangent and double exponential models in the fixed-bed column, Sep. Purif. Technol. **212** (2019) 572.
doi: https://doi.org/10.1016/j.seppur.2018.11.071
68. *Rodriguez-Acosta, J. W., Mueses, M. Á., Machuca-Martínez, F.,* Mixing rules formulation for a kinetic model of the Langmuir-Hinshelwood semipredictive type applied to the heterogeneous photocatalytic degradation of multicomponent mixtures, Int. J. Photoenergy **2014** (2014) 817538.
doi: https://doi.org/10.1155/2014/817538